Mixed Systems of Tethered Chains in Spherical Volumes. A Model for Cores of Mixed Copolymer Micelles

Zuzana Limpouchová, David Viduna, and Karel Procházka*

Department of Physical and Macromolecular Chemistry, Faculty of Science, Charles University in Prague, Albertov 2030, 128 40 Prague 2, Czech Republic

Received January 2, 1997; Revised Manuscript Received July 21, 1997[⊗]

ABSTRACT: Conformations of tethered chains enclosed in small spherical cavities were studied by computer simulations at high segment densities. The systems studied contain two types of compatible chains that mutually differ in length. They have been studied as models for cores of mixed multimolecular block copolymer micelles in selective solvents. Simulations were performed on a tetrahedral lattice using (i) mutually independent simultaneous self-avoiding growth of all chains, and (ii) modified equilibration algorithm similar to that of Siepmann and Frenkel [Siepmann, J. I.; Frenkel, D. *Mol. Phys.* **1992**, *75*, 59]. Only the geometric exclusion effect of segments was considered since it plays a dominant role in dense systems. It has been found that the systems studied are very disordered and the short chains in mixed systems decline more from the radial direction than the long chains. The distribution functions of pair distances of free ends of short and long chains in mixed systems significantly differ from each other. This fact is very important for interpretation of results of fluorometric studies on mixed systems. When a low fraction of tagged chains, which differ significantly in length from the nontagged chains, are added to the original system to get a fluorescently active micellar system, fluorometric measurements do not yield information on the original system, but information on conformations of added chains only.

Introduction

Block copolymers AB and ABA self-associate in dilute solutions in selective solvents (a good solvent for block A and poor for B) and form spherical multimolecular micelles.[1] Block copolymer micelles consist of compact spherical cores formed by insoluble blocks, B, and protective shells formed by soluble blocks, A. Micellization of block copolymers obeys the scheme of reversible closed association,[2] characterized by the equilibrium between unimers, i.e., non-associated chains (U) and micelles (M)

$$n\mathrm{U} \overset{K}{\rightleftharpoons} \mathrm{M} \qquad (1)$$

where n is the association number, which is for typical micellizing copolymers in the range 10^1-10^2, and K is the micellization equilibrium constant. Multimolecular micelles are usually fairly monodisperse in mass and size and are very small for their particle molar mass due to the compactness of the core. Micellization equilibrium is often strongly shifted in favor of micelles and the equilibrium concentration of unimers is therefore very low.

Micellization equilibrium in copolymer solutions is controlled by the complex and very sensitive entropy-to-enthalpy balance of the whole system and the thermodynamic description of the behavior of micellar solutions of high molar mass copolymers is a difficult and challenging problem. A considerable number of papers have been published on that subject.[3] The existing theories are able to predict the general behavior of micellizing copolymers fairly well. However, not all properties of micellar systems have been explained in detail.

In recent years, micellization of detergents and low molar mass copolymers has been studied by molecular dynamics[4] and by Monte Carlo computer-based simulations.[5] The studies were mainly aimed to prove the spontaneous association of chains in strongly selective solvents. From the methodological point of view, they represent excellent pieces of work. However, only relatively short chains were studied due to the complexity of the problem, and the performed simulations did not, therefore, yield detailed and sufficient information on conformations of blocks in micellar cores and shells.

Studies of chains tethered to curved surfaces is another approach that allows for conformational analysis of core-forming and shell-forming blocks. This approach is less general; however, it is very fruitful, mainly if particular or highly specific problems are studied. Important information on tethered chain conformations at high densities has been obtained by Monte Carlo and molecular dynamic simulations,[6] by self-consistent field theories[7] and also by experimentalists.[8] In spite of the intense interest of theoreticians in systems of tethered chains, the behavior of mixed systems enclosed in small volumes has been studied relatively little.[7h] Knowledge of the behavior of such systems may help to understand formation of mixed micelles composed either of copolymers differing in chemical structure and composition of blocks or of couples of copolymers of the same type that differ in the length of blocks. Only few experimental papers have been published[9] on the subject.

In our earlier papers,[9c,d,10] we have studied homogeneous and mixed micellar systems using various experimental techniques, mainly ultracentrifugation and a combination of light scattering with steady-state and time-resolved fluorometry. The time-resolved fluorometry studies were aimed at yielding information on the space distribution of pendant fluorophores in micellar cores and on conformations and segmental dynamics of core-forming blocks.[10] In this paper, we study tethered chain conformations in binary systems composed of short and long compatible chains in small spherical cavities (a model for cores of mixed micelles) by Monte Carlo computer simulations. Reliable knowledge of insoluble block conformations in micellar cores is needed for the correct interpretation of results of fluorometric

* To whom correspondence should be addressed. E-mail: prochaz@vivien.natur.cuni.cz.

[⊗] Abstract published in *Advance ACS Abstracts,* November 15, 1997.

S0024-9297(97)00001-6 CCC: $14.00

measurements. Simulations of processes of nonradiative excitation energy transfer and migration among end-attached fluorophores in micellar cores will be reported in our next papers.

Method

Simulation Technique. Dense systems of self-avoiding chains enclosed in a small spherical cavity and tethered by one end to the surface of the cavity have been studied by Monte Carlo simulations. Conformations of N_1 tethered chains (of the shorter length, L_1) and N_2 tethered chains (of the longer length, L_2) enclosed in a spherical volume were obtained by the mutually independent simultaneous self-avoiding random walk (SAW) of all $(N_1 + N_2)$ chains on a tetrahedral lattice, together with the careful equilibration of the system in a spherical cavity with the radius, $R = 10l$, (containing ca. 2800 lattice sites, l is the lattice distance). Physical relevance of this model for micellar cores will be discussed in the Results and Discussion.

Simulations of multichain arrangements and the subsequent "thermal equilibration" of the system have been described in our earlier papers.[11] A modified algorithm, which is suitable for generation of chain conformations in mixed dense systems, was performed in several steps:

(i) The spherical cavity of a given radius, R, is defined on a tetrahedral lattice. The first segments of all $N = N_1 + N_2$ chains, i.e., the tethered segments, are placed at random into a narrow spherical surface layer of the thickness, $\Delta r_{\mathrm{Surf}} = 0.1l$ (ca. 170 surface lattice sites for $R = 10l$). The only limitation is that none of the mutual distances between tethered ends can be less than a certain limit, $1.5l-4.0l$ (depending on the total number of all chains), to get a relatively uniform surface density of tethered ends. Then the mutually independent simultaneous self-avoiding growth of all chains takes place in the cavity. All chains, $l = 1, ..., N$, are one by one prolonged in each step, k, by one segment. The biased sampling that takes into account only the unoccupied lattice sites is used.

(ii) If an intersection of two chains occurs in the kth step of the simultaneous growth of chains, the intersecting chain, l, is disregarded and a new chain is grown from a new randomly chosen surface site up to the kth step. Then the further simultaneous growth of all chains continues from the $(k + 1)$th step.

(iii) If the remedy (ii) fails many times, i.e., if a generation of 3×10^4 random segment positions does not produce a nonintersecting system in the kth step of the simultaneous growth of all chains, a random integer number $i \in \langle 1, 4\rangle$ is generated, and all chains are cut by i steps and a simultaneous random self-avoiding growth of all chains starts from the $(k - i)$th step.

A combination of steps i−iii continues until a nonintersecting micellar core containing NL_1 segments is produced. Since the used simulation procedure is fully random, it may happen that a very inhomogeneous system (with very tightly packed regions) is yielded during the simulation. It seriously hinders the further growth of chains and it is more efficient to start a new self-avoiding growth of all chains from the very beginning. This is done if a complete nonintersecting system of NL_1 segments is not obtained on the basis of 10^5 random numbers. At high densities, the simulation efficiency is generally very low (e.g., for the fraction of occupied lattice sites ca. 0.7, the yield of accepted segment positions in equilibrated micellar cores, expressed as the ratio of accepted to all generated segment positions, is only ca. 0.1%). To accelerate the simulation procedure, we have used a modified algorithm that we had developed and tested earlier.[11] In this fast version, the simultaneous self-avoiding walk of N shorter chains containing either L_1 or even a slightly lower number of segments is performed first. Created tethered chains in a nonintersecting system are prolonged up to the required lengths L_1 and L_2 prior to the equilibration procedure, which is performed in three steps:

(iv) A random chain is disregarded, and a new chain grows from a randomly chosen surface position in the dense system. This procedure is used to remove the larger part of the nonphysical contribution caused by the continuously growing density of the system in the previous step. This procedure is repeated N^2 times. Both short and long chains are grown independently.

(v) The final equilibration is performed to correct the biased sampling:[12] A random chain is disregarded and a new chain of the same length is grown again from a random surface site. Since only the unoccupied lattice sites are *a priori* considered for the self-avoiding growth of individual chains, the biased sampling must be corrected: The Rosenbluth weights,[13] $w_1^{(k)}$, are calculated in each step, k, during the growth of the lth chain. Then the total weight of the lth chain is evaluated, $W_1 = \Pi_{(k)} w_1^{(k)}$, and a modified acceptance criterion of the Metropolis type[14] is applied either to accept or to refuse the new chain. A random number, $X \in \langle 0, 1\rangle$ is generated[15] and the new chain is accepted if the following nonequality is fulfilled, $X \leq W_{\mathrm{new}}/W_{\mathrm{old}}$. Our algorithm is based on the Monte Carlo variant proposed by Siepmann and Frenkel[16] for dense polymer melts. Chains are replaced at random. They grow mutually independently in the dense medium and they are statistically uncorrelated. Step v is repeated until N^2 new chains are accepted and the system formed by last N accepted chains is considered as one random micellar core. Since all equilibrated multichain systems have been created independently from each other, all of them may be used for evaluation of conformational characteristics of tethered chain systems.

During the equilibration of the multichain system, one randomly chosen chain only is disregarded in a given time and only one new chain may grow on the lattice that is occupied by segments of the remaining $(N - 1)$ original chains. The actual density increase during the growth of the new chain is in the region $0.01-0.03$ depending on the combination of N and L, which is a quite negligible change for simulations at densities ca. 0.55. Despite the fact that all chains grow sequentially from their tethered ends, the method used should not produce an appreciable systematic effect, resulting in a nonphysical contribution to the difference in the behavior of tethered and free ends. To check for and to correct (if necessary) a possible influence of the sequential self-avoiding walk of all chains from the tethered end, we have recently included a new equilibration step that had not been used in our early simulations. The optimized variant of the supplementary equilibration step is the following:

(vi) A random chain is disregarded and grows again from a random unoccupied lattice site anywhere in the sphere. It means that the self-avoiding growth starts from a random middle segment (k) of the chain. When the $(k + i)$th segment reaches the surface, a random number $\xi \in \langle 0, 1\rangle$ is generated. If $\xi \leq 1/2$, then the $(k + i)$th segment is considered as the tethered end of the

new chain, and the other part of this chain is grown from the kth segment. If $\xi > 1/2$, then the situation is regarded as a close approach of the chain to the impermeable surface and the growth continues inside the sphere. If the tethered end is not created within L steps, then the chain is disregarded and a new chain is grown from a new random position k'. The Rosenbluth weights are evaluated for individual chains and the Metropolis-like acceptance criterion is applied similarly to the previous case.

Conformational characteristics were evaluated for several systems on the basis of (a) the two and (b) the three above described equilibration steps and mutually compared. Differences were in the range of random errors of stochastic simulations, which indicates that the second equilibration step alone produces fairly equilibrated systems. Since the supplementary equilibration does not affect the data (but it prolongs significantly the simulation time), the published data are based on the two-step equilibration only.

All attempts to employ an independent equilibration algorithm based on local moves (in order to check if the equilibrium systems have been created) failed since it was impossible to equilibrate the system in acceptable times (the ratio of accomplishable to the attempted moves at high densities was below 10^{-4}). It was the main reason why the Siepmann and Frenkel algorithm was used since it works well up to very high densities.

The calculated distribution functions are based on 2×10^4 equilibrated cores, which represents a total number of $10^{10}-10^{11}$ of all generated segment positions, i.e., positions that were either accepted or refused (since they did not lead to noncolliding systems or were not accepted on the basis of the Metropolis rule). Calculations were performed on a workstation INDY XL-8 R4600SC/133 MHz, Silicon Graphics, Inc. Programs were written in FORTRAN 77. The longest calculations took up to 2 months of the CPU.

Results and Discussion

Behavior of multicomponent systems of micellizing block copolymers in selective solvents depends considerably on the ability of copolymer samples to form mixed micelles. The thermodynamic stability of mixed micellar cores is *primus inter pares* among important factors that control formation of mixed micelles. Due to the incompatibility of polymer chains that differ significantly in chemical nature, formation of mixed block copolymer micelles with chemically different insoluble blocks has never been observed. On the other hand, it is a well-established fact that strongly polydisperse samples (differing in lengths of blocks) form micelles that are fairly monodisperse in mass and size.[1]

Before we attempt to discuss the data, we would like to address the question of the direct physical relevance of the model system for cores of realistic block copolymer micelles. Since all junctions of soluble and insoluble blocks in multimolecular micelles in a strong segregation regime are localized in a narrow spherical interfacial region, a system of chains enclosed in a small spherical region and tethered by one end to the surface is a generally correct model system for micellar cores.

Since properties of dense polymer systems are determined mainly by repulsive forces, athermal systems that take into account only the geometric excluded effect of segments have been studied in this paper. Although a system of self-avoiding chains without other interactions may seem very simplistic, it captures all important features of the behavior of flexible chains at high densities. The choice of this model system simplifies and accelerates the simulation procedure, and computer studies at very high densities are therefore feasible despite the fact that they are still very time-consuming. However, there is another reason for studying a well-defined and very simple system first: Constrained systems of tethered chains behave unlike other polymer systems. A proper knowledge of the behavior of a reference system is therefore needed. This knowledge will allow us to differentiate between general properties of constrained tethered chains and additional effects caused by interactions, etc. The system containing flexible chains that experience only the geometric excluded effect of segments is a good reference system, and analogical systems, e.g., hard spheres,[12a] are frequently used as reference systems in statistical thermodynamics of fluids.

In our earlier papers[11] we have shown that Monte Carlo simulations on dense systems of tethered chains enclosed in small spherical volumes yield important information on conformations of core-forming blocks in multimolecular micelles. However, our simulation technique does not allow us to optimize the micellar structure and great care and precaution has to be devoted to the interpretation of the data. In order to minimize the risk of incorrect conclusions, we have performed a series of simulations in a broad range of segment densities.[11e] For each density, we have studied several systems differing in combination of numbers of chains, N, and their length, L. Computer simulations showed that the basic shape of various distribution functions depends neither on segment density (i.e., on the product of NL) nor on actual values of N and L for segment densities higher than 0.25. This finding suggests that the model studied describes the conformational behavior of insoluble blocks in micellar cores differing in the degree of swelling reasonably well (at least at the semiquantitative level).

In the region of low densities, the shapes of individual distribution functions differ considerably from those obtained at high densities. These systems do not correspond to micellar cores but provide information important for understanding the behavior of dilute systems of end-adsorbed chains in spherical pores. There exist a number of theoretical and experimental papers on polymer chains in pores or in constrained geometries.[17] Most of them are aimed at calculating the conformational entropy of the enclosed or adsorbed chains that is necessary for evaluation of the partition coefficient. This paper deals with dense systems. More data on dilute polymer systems enclosed in spherical cavities (tethered as well as untethered) and the appropriate discussion will be published in the future.

To get maximum information on mixed micelles, we have performed simulations on several model systems differing in numbers of chains and their lengths. Parameters of the system studied are given in Table 1. Systems with $N_1/N_2 = 15/15$ were studied most thoroughly. They were chosen to show the most typical features of mixed systems. The average chain length, L_{av}, equals 50 and the components differ by $\Delta L = 0$ (the homogeneous reference system), 20, 40, and finally 60. The average segment density, $\langle g_s \rangle = 0.55$, as well as the number fractions of chains, $x_i = 0.5$, are constant in systems with $N_1/N_2 = 15/15$; however, the weight fraction of longer chains, w_2, increases ($w_2 = 0.5$, 0.6, 0.7, and 0.8). Systems with a considerable surplus of

Table 1. Parameters of the Studied Systems[a]

N_2/L_2	N_1/L_1	ΔL	L_{AV}	x_1	x_2	w_1	w_2	g_s
15/80 (7)	15/20 (1)	60	50 (11)	0.5	0.5	0.2	0.8	0.55
15/70 (6)	15/30 (2)	40	50 (10)	0.5	0.5	0.3	0.7	0.55
15/60 (5)	15/40 (3)	20	50 (9)	0.5	0.5	0.4	0.6	0.55
15/50 (4)	15/50 (4)	0	50 (8)	0.5	0.5	0.5	0.5	0.55
5/180 (2)	25/24 (1)	156	50	0.17	0.83	0.4	0.6	0.55

[a] Symbols used: N_1/L_1, number of shorter chains/their length in segments; N_2/L_2, number of longer chains/their length in segments; ΔL, difference in lengths between longer and shorter chains; L_{AV} average chain length; $x_i = N_i/(N_1 + N_2)$, number fraction of chains i; $w_i = N_iL_i/(N_1L_1 + N_2L_2)$, weight fraction of chains i; g_s, segment density: The number in the parentheses gives the appropriate numbering of curves in Figures 1, 2, and 4−8.

either short or long chains (i.e., systems with $N_1/N_2 = 5/25$ and $N_1/N_2 = 25/5$) were studied since similar systems are often investigated by fluorometry: In fluorescence measurements, it is often necessary to "dilute" the tagged chains with the nontagged ones to suppress the energy transfer. In experimental studies, it is not always possible to guarantee equal lengths of tagged and nontagged chains, and thus, mixed micellar systems differing in lengths of blocks and differing also due to tagging are studied instead of monodisperse systems.

Systems studied by computer simulation are appreciably smaller that those studied experimentally. A relatively small size of the studied system is the necessary condition for practically feasible computer studies. Recently, we have performed three extremely time-consuming simulations for almost realistic micellar cores in order to establish a direct relation to real micellar systems (approximately 2 months of CPU time at the INDY workstation). Real micelles that we have studied by light scattering and fluorometric techniques in aqueous media[10b−e] are composed typically of ca. 10^2 copolymer chains, and the length of the insoluble polystyrene block ranges from 10^4 to 3×10^4 g/mol, which represents a hundred to a few hundreds of monomeric units. The density of the core in 1,4-dioxane−water (30−40 vol %) mixtures, in which micelles form spontaneously, is ca. 0.5−0.6 g/mL, while the density of the amorphous polymer is ca. 1.0 g/mL. To get comparable simulated systems, the following numbers of chains of the lengths $L = 160$ were used: $N = 100$, 150, and 200 in the cores of the radius, $R = 21.5l$, $24.5l$, and $27l$. Systems based on the above given numbers lead to the average density of the occupied lattice sites on the tetrahedral lattice 0.6. This choice should guarantee almost the same significance of geometrical constrains in simulated and experimentally studied systems (the similar fractions of occupied lattice points as the ratio of experimental densities of swollen cores and the amorphous polymer). From semiquantitative point of view, the results of simulations are essentially the same as those for smaller systems and may be provided upon request.

Segment Densities. When considering mixed micellar cores formed by blocks that differ appreciably in length, one *a priori* expects a higher density of segments of longer blocks than that of shorter blocks in the central part of the core. We have found in our earlier studies[11] that the core-forming blocks in homogeneous systems are fairly disordered. If both types of blocks are long enough, the reasons for the aforementioned difference in local densities is no longer evident. It is therefore interesting to compare segment densities of short, $g_S^{(1)}(r)$, and long chains, $g_S^{(2)}(r)$, as functions of the

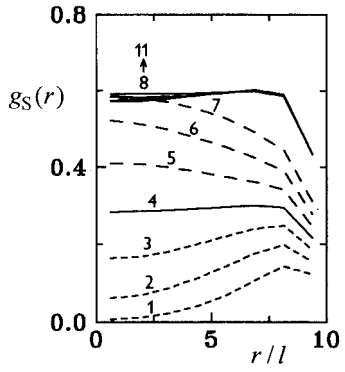

Figure 1. Segment densities $g_S^{(1)}(r)$, $g_S^{(2)}(r)$, and $g_S(r)$ as functions of the distance from the center of the spherical cavity with the radius, $R = 10l$, for dense systems composed of 15 longer and 15 shorter chains at the average segment density 0.55. Segment densities, $g_S^{(1)}(r)$, of shorter chains with the length $L = 20$, 30, and 40 are represented by dashed curves 1−3 with short dash marks, and segment densities, $g_S^{(2)}(r)$, of longer chains with $L = 60$, 70, and 80 are represented by dashed curves 5−7, with long dash marks. Couples of curves 3 and 5, 2 and 6, and 1 and 7 correspond to three systems with $\Delta L = 20$, 40, and 60. Full curve 4 shows the segment density of half of the chains in the homogeneous reference system with the average length, $L = 50$ (i.e., density of 15 chains that represent "one component"). Full curves 8−11 show total segment densities, $g_S(r)$, for systems with $\Delta L = 0$, 20, 40, and 60.

distance from the core center for several systems of chains with increasing difference in the chain length, $\Delta L = L_2 - L_1$. The calculated functions are proportional to the experimental segment densities (in g·cm^{-3}) that can be measured by a combination of small angle X-ray scattering (SAXS) and small angle neutron scattering (SANS) in mixed deuterized/nondeuterized micellar systems.

It is evident from Figure 1 that the density of segments of longer chains, $g_S^{(2)}(r)$, does really increase (dashed curves 5−7, with long dash marks) and the density of shorter chains, $g_S^{(1)}(r)$, decreases toward the core center (dashed curves 1−3, with short dash marks). This effect is fairly pronounced for large differences, ΔL. Combination of two curves, i.e., couples: 1 and 7, 2 and 6, and 3 and 5 describe three individual mixed systems. The full curve 4 corresponds to the system composed of chains that do not differ in length (i.e., to the homogeneous reference system). The full curves 8−11 show the total average densities of mixed systems. The total density, $g_S(r)$, is almost constant for all studied systems which is in agreement with experimental (SAXS/SANS) data.[18] A sudden drop in the simulated data close to the surface is due to strong geometrical constraints imposed by the surface. In real micellar systems, segments of soluble and insoluble blocks are partially intermixed in the interfacial region, and the density of core-forming blocks also decreases in this narrow layer. The observed behavior of individual chains looks straightforward; however, it is a result of fairly complex behavior of the whole system, which may be understood if the behavior of other simulated conformational characteristics is taken into account.

Figure 2 shows the density of the free chain ends, $g_F^{(i)}(r)$, for the same systems as in Figure 1 (the curves for the system with $\Delta L = 20$ have not been included to gain a clear and comprehensive figure). In mixed systems, the density rises toward the core center for long and medium chains and decreases for short chains. The density of free ends of longer chains is systematically higher in the central part of the sphere than that of

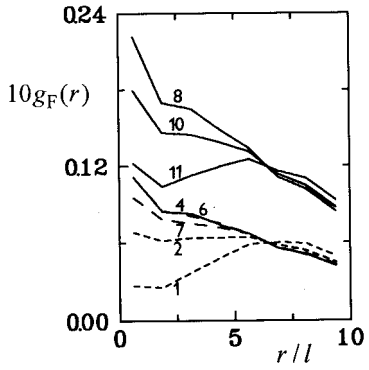

Figure 2. Densities of free ends, $g_F^{(1)}(r)$, $g_F^{(2)}(r)$, and $g_F(r)$ for the same systems as in Figure 1. Curves 3, 5, and 9 are not shown to gain a comprehesive figure.

short chains and changes relatively little with increasing length. Values of $g_F^{(2)}(r)$ surprisingly slightly decrease with increasing ΔL in the central region of the sphere, i.e., for low r. Curves for short chains show a significant decrease in the central part of the sphere and the total density of free ends also shows a pronounced minimum in the central region for systems with large differences in L. A certain scatter in simulated values for $r \rightarrow 0$ is due to the worse statistics of simulated data as compared with that for higher values of r (fluctuations are due, in major part, to very low numbers of the lattice sites that come into account for small r and, in minor part, to lower number of the end segments as compared with the total number of all chain segments).

Conformations of Individual Chains. Functions that describe angular orientations of chains with respect to the radial direction yield important information on the conformational behavior of tethered chains in spherically symmetrical systems. Two functions of that type are presented in this communication: (a) the distribution function of orientations of tethered-to-free end vectors, $\mathbf{r}_{TF}$, with respect to the radial direction, $\mathbf{r}$, (defined from the tethered end of a particular chain to the core center), $\psi^{(r)}{}_{TF}(\varphi)$, and (b) distribution of orientations of tethered end-to-gravity center vectors, $\mathbf{r}_{TC}$, with respect to the radial direction, $\psi^{(r)}{}_{TC}(\varphi)$. Both functions are the probability densities, and they are constructed as histograms during the computer simulations. The first one is related to the fraction of chains with their free ends placed in narrow volumes confined between two cones with the common apex located in the tethered end, $n^{(r)}{}_{TF}(\varphi)$. The apex angle of the inner cone is 2φ and that of the outer cone is $2(\varphi + \Delta\varphi)$, with $\Delta\varphi = 5°$, see the two-dimensional schematics in Figure 3 (the narrow interconical volumes are obtained by rotating the corresponding angular differences $\Delta\varphi$ around the radial direction). Numbers of chains, $N^{(r)}{}_{TF}(\varphi)$, that are obtained during the simulation procedure are averaged over all tethered ends and normalized by numbers of chains *per* one micelle (in this way, number fractions, $n_{TF}{}^{(r)}(\varphi)$, are obtained) and further divided by numbers of all lattice sites in appropriate interconical volume elements, N_φ. Normalization numbers, N_φ, are averaged over all surface lattice sites (possible locations of tethered ends of chains in a narrow surface layer of the thickness $\Delta r_{Surf} = 0.1l$). The last averaging procedure is necessary since we use a combination of the spherical cavity and the tetrahedral lattice and N_φ depend slightly on the apex position in the surface layer with respect to the fixed system of coordinates. Since we have been using relatively complicated symbols for calculated

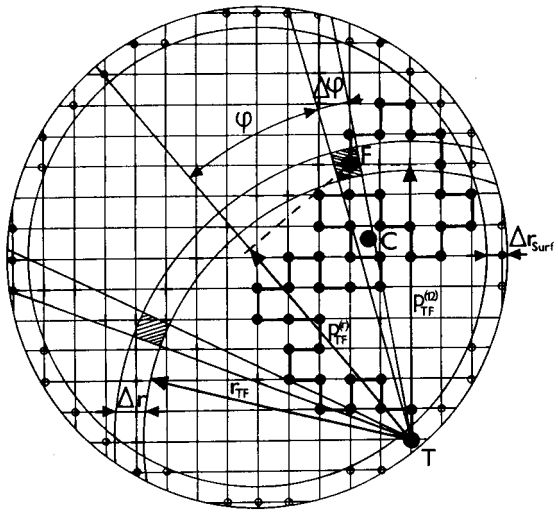

Figure 3. Two-dimensional schematics explaining the evaluation and normalization procedure used to calculate conformational characteristics for systems of tethered chains in closed spherical volumes.

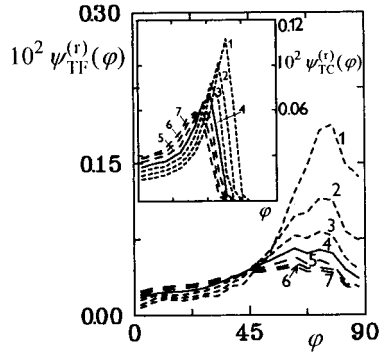

Figure 4. Angular distribution functions of orientations of tethered end-to-free end vectors, $\mathbf{r}_{TF}$, with respect to the radial direction, $\psi^{(r)}_{TF}(\varphi)$, for the same mixed systems of short and long chains as in Figure 1. Insert: Corresponding angular distribution functions of orientations of tethered end-to-gravity center vectors, $\psi^{(r)}_{TC}(\varphi)$.

functions, we have omitted in this paper superscript $i = 1, 2$ for short and long chains, respectively, in all cases when it cannot confuse the reader. Curves for short and long chains are mutually distinguished by different lengths of the dash marks, and they are properly described in figure captions.

Figure 4 shows distribution functions $\psi^{(r)}{}_{TF}(\varphi)$ for the same systems as in Figure 1. General shape of these curves, which cannot be explained on the basis of simplified geometrical considerations, was discussed and explained in our earlier papers.[11b,d] It has been shown that it is the result of the maximum entropy principle in constrained systems with a high and spatially constant density. The whole space has to be filled in homogeneously with chain segments, and simultaneously, the maximum number of possible chain conformations must be reached in the macroscopic ensemble of micelles. The most striking feature of the behavior of mixed systems is the following: Orientations of end-to-end vectors of short chains decline on average more from the radial direction than those of long chains. Maxima in $\psi^{(r)}{}_{TF}(\varphi)$ curves for shorter chains (curves 1−3, with short dash marks) are more pronounced, and their positions are shifted to larger φ with decreasing chain length. A concomitant decrease in $\psi^{(r)}{}_{TF}(\varphi)$ values for small φ is also observed. The distribution functions for long chains (curves 5−7, with long dash-marks) are

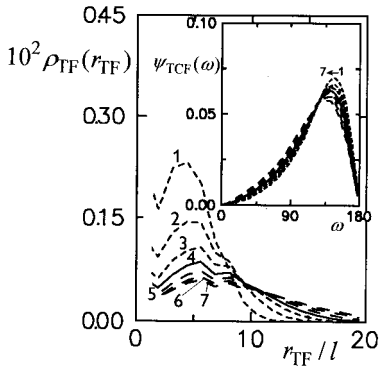

Figure 5. Distribution functions of tethered-to-free end distances, $\rho_{TF}(\mathbf{r}_{TF})$, for the same systems as in Figure 1. Insert: Angular distribution functions $\Psi_{TCF}(\omega)$ of mutual orientations of $\boldsymbol{r}_{TC}$ and $\boldsymbol{r}_{FC}$ vectors for the same systems.

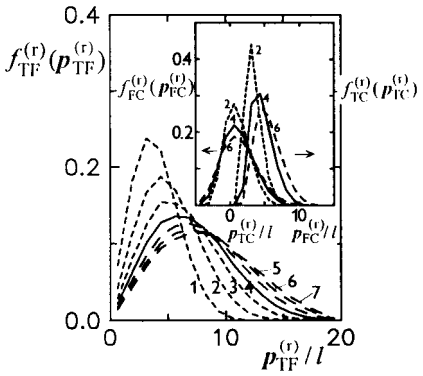

Figure 6. Distribution functions of projections of $\mathbf{r}_{TF}$ vectors into the radial direction, $f_{TF}^{(r)}(\boldsymbol{p}_{TF}^{(r)})$, for the same systems as in Figure 1. Insert: Distribution function of projections of tethered end-to-gravity center vectors, $f_{TC}^{(r)}(\boldsymbol{p}_{TC}^{(r)})$, and free end-to-gravity center vectors, $f_{FC}^{(r)}(\boldsymbol{p}_{FC}^{(r)})$, for the homogeneous system with $\Delta L = 0$ and the mixed system with $\Delta L = 40$. Numbering of curves corresponds to Figure 1.

broader, and their maxima are less pronounced as compared with those for shorter ones. Very similar, but even more pronounced, trends in the curve shapes are shown in the insert, where the corresponding distribution functions describing the orientation of the tethered end-to-gravity center vectors, $\mathbf{r}_{TC}$, are depicted. One observes a fairly obvious increase in aberration of the most probable tethered end-to-gravity center vector orientations with decreasing chain length. Systematic changes in $\psi^{(r)}{}_{TC}(\varphi)$ values at low angles φ are also obvious.

The slightly unexpected behavior of mixed micellar cores shown in Figure 4 may be rationalized and explained as follows: Tethered chains are placed in a restricted volume that they have to fill in homogeneously. The effective flexibility of tethered chains in closed spherical cavities is considerably reduced as compared with corresponding free chains and depends mainly on the behavior of small and relatively stiff parts of the chain that are forced to turn to match the cavity. The "true stiffness" of the chain decreases from the tethered end toward the free one (see also papers in ref 11). For this reason, a high fraction of short chains has to start in an oblique direction from the tethered end to fill in a large subsurface layer. Long chains may later turn toward the center of the sphere more easily (i.e., in several "smaller turns") than the short ones. It results in a broader shape of functions $\psi^{(r)}{}_{TF}(\varphi)$ and $\psi^{(r)}{}_{TC}(\varphi)$ for longer chains with a lower maximum value at a lower angle φ and consequently also in the above mentioned increase in $g_S^{(2)}(r)$ values in the central region (see Figure 1).

Figure 5 shows the normalized distribution functions of tethered end-to-free end distances of individual chains, r_{TF}, i.e., functions $\rho_{TF}(r_{TF})$, for the same systems as in Figure 1. Function $\rho_{TF}(r_{TF})$ represents the probability density that the free end of a chain is placed in the distance r_{TF} from its tethered end, which is placed randomly in a narrow spherical surface layer of the thickness $\Delta r_{Surf} = 0.1l$. Functions $\rho_{TF}(r_{TF})$ are calculated as follows: The average numbers of the free ends of chains in the distance (r_{TF}, $r_{TF} + \Delta r$) from their tethered ends (in one micellar core) are normalized by numbers of chains forming one core and by numbers ΔN_r of all lattice sites in narrow semispherical layers (r_{TF}, $r_{TF} + \Delta r$), with $\Delta r = 1.25l$ (see schematics in Figure 3). Similarly to the evaluation of angular distribution functions, numbers ΔN_r are averaged over all possible locations of the tethered ends of chains, i.e., over all surface lattice sites. Number fraction of chains with particular r_{TF} distances, $n_{TF}(r_{TF})$ (not normalized by numbers ΔN_r), corresponding to individual curves $\rho_{TF}(r_{TF})$ are not shown since they may be recalculated from $\rho_{TF}(r_{TF})$.

Angular distribution functions $\psi_{TCF}(\omega)$, are shown in the insert in the Figure 5. They describe the probability of mutual orientations of two following vectors: (i) the gravity center-to-tethered end vector, $\mathbf{r}_{TC}$, and (ii) the gravity center-to-free end vector of the same chain, $\mathbf{r}_{CF}$. Changes in the most probable TCF angle, ω, are very small; nevertheless, they are systematic. An average contour of the chain resembles an open letter "C" with the most probable angle ca. 140−150°. However, chains with angles TCF from 90 to 170° are in all cases quite abundant.

In our earlier studies for homogeneous systems,[11] we have shown that the "free halves" of chains are more flexible and more coiled than the "tethered halves". They recoil into almost all directions with respect to the chain beginning, and a nonnegligible fraction of chains recoil back and the free ends may come quite close to their tethered ends. This conclusion is also obvious from the analysis of various conformational characteristics of mixed systems, and it may be also deduced from shapes of the three following functions that describe distributions of projections $\mathbf{p}_{ij}^{(r)}$ of vectors $\mathbf{r}_{TF}$, $\mathbf{r}_{TC}$, and $\mathbf{r}_{FC}$, into the radial direction, i.e., functions $f_{TF}^{(r)}(\mathbf{p}_{TF}^{(r)})$, $f_{TC}^{(r)}(\mathbf{p}_{TC}^{(r)})$, and $f_{FC}^{(r)}(\mathbf{p}_{FC}^{(r)})$, respectively. Functions $f_{TF}^{(r)}(\mathbf{p}_{TF}^{(r)})$ are shown in Figure 6 for the same systems as in Figure 1 and the two other functions, $f_{TC}^{(r)}(\mathbf{p}_{TC}^{(r)})$ and $f_{FC}^{(r)}(\mathbf{p}_{FC}^{(r)})$, are depicted in the insert, however, only for the homogeneous reference system and one mixed system with the difference, $\Delta L = 40$ in order to get a comprehensive figure. The shape of $f_{FC}^{(r)}(\mathbf{p}_{FC}^{(r)})$, with the maximum close to $\mathbf{p}^{(r)}{}_{FC} = 0$, supports the above mentioned conclusion concerning the important fraction of "free halves" of chains (even of very short ones) that recoil back toward their tethered ends. Functions $f_{FC}^{(r)}(\mathbf{p}_{FC}^{(r)})$ are slightly broader for longer chains, but they are affected only a little by the fact if the chain of a given length is in a homogeneous[11] or a mixed system.

Pair Distribution Function of Mutual Distances of Free Ends of Chains. The most important function for interpretation of fluorometric measurements with the end-tagged copolymers is the pair distribution function of mutual distances of free ends of chains of the type i and j, $\rho_{FF}^{(ij)}(r_{FF})$ Functions $\rho_{FF}^{(ij)}(r_{FF})$ that we

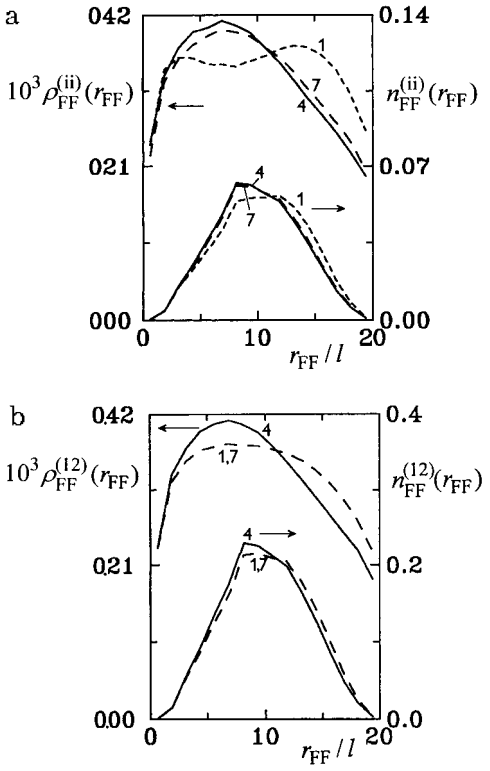

Figure 7. (a) Normalized pair distribution functions of mutual distances of free ends of chains, $\rho_{FF}^{(ii)}(r_{FF})$, and the corresponding nonnormalized number fractions, $n_{FF}^{(ii)}(r_{FF})$, for systems with $\Delta L = 0$ (solid curves) and 60 (dashed curves). (b) Distribution functions of mutual distances of free ends of short and long chains, $\rho_{FF}^{(12)}(r_{FF})$ and $n_{FF}^{(12)}(r_{FF})$, for the same systems as in Figure 7a. Numbering of curves corresponds to Figure 1 except that the curves marked by 1,7 mean the cross-correlation functions between groups of chains 1 and 7 in Figure 7a.

present in our communication are relative distribution functions normalized *per* one pair of ends of the type (1-1), (2-2), and (1-2), respectively, and they are further divided by the distribution function of mutual distances of pairs of the lattice sites in the cavity. The used normalized functions, $\rho_{FF}^{(ij)}(r_{FF})$, have the following advantage: They would be constant and independent of r_{FF} for fully random distribution of free ends (or fluorophores that are covalently attached at the ends of blocks). Any curvature is the clear indication of a nonrandomness in the spatial distribution of free ends (the end-attached fluorophores) and it allows for discussions of the fluorescence and anisotropy decays.

Simulated functions $\rho_{FF}^{(11)}(r_{FF})$ for short chains, and $\rho_{FF}^{(22)}(r_{FF})$ for long chains are shown in Figure 7a for systems with $\Delta L = 0$ and 60 together with the corresponding number fractions $n_{FF}^{(ii)}(r_{FF})$, i.e., with functions that are not normalized by the distribution of the lattice sites distances. The cross-correlation functions, $\rho_{FF}^{(12)}(r_{FF})$ and $n_{FF}^{(12)}(r_{FF})$, describing the distribution of pair distances between ends of short and long chains, are shown in Figure 7b.

Simulated curves for all systems suggest that the distribution of end tags is generally nonrandom. Curves for long chains are similar to those for homogeneous systems composed of medium or long chains.[11a,e] Curves for shorter chains in the mixed systems are different—these curves show shallow minima for medium r_{FF} values. These shapes may be understood with the help of curve $g_F^{(l)}(r)$ (see Figure 2), which shows that

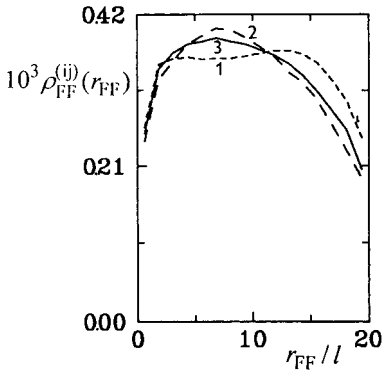

Figure 8. Normalized pair distribution functions $\rho_{FF}^{(ii)}(r_{FF})$ in the system composed of 5 chains of the length $L = 180$ and 25 chains of the length $L = 24$: function $\rho_{FF}^{(11)}(r_{FF})$ for short chains (dashed curve 1), function $\rho_{FF}^{(22)}(r_{FF})$ for long chains (dashed curve 2), and distribution function of mutual distances of ends of short and long chains $\rho_{FF}^{(12)}(r_{FF})$ (fill curve 3).

short chains do not often reach into the central part of the sphere. Free ends of short chains are fairly abundant in a layer ($r \approx 5l-9l$) close to the surface. Due to the spherical shell-like shape of this region, short and long distances between pairs of free ends are more frequent.

General Comments Concerning Systems with a Considerable Surplus of One Component. Systems containing a small fraction of chains that differ considerably in the length from those that are in a great majority in the mixed system are often studied by fluorescence techniques. Simulations indicate that characteristics describing conformations of individual tethered chains do not almost depend on the number fractions of chains in the mixture, and they are not shown here. However, functions describing mutual orientations of different chains do. Figure 8 shows functions $\rho_{FF}^{(11)}(r_{FF})$, $\rho_{FF}^{(22)}(r_{FF})$, and $\rho_{FF}^{(12)}(r_{FF})$ for a system composed of 25 short and 5 long chains ($L_1 = 24$, $L_2 = 180$). Properties of the whole system resemble to the homogeneous system composed of short chains;[11e] however, functions $\rho_{FF}^{(11)}(r_{FF})$ and $\rho_{FF}^{(22)}(r_{FF})$ differ appreciably from each other.

The last mentioned finding is very important for fluorometric studies. It shows that data on systems containing tagged and nontagged chains have to be interpreted with great care. If a mixed micellar system is prepared from a very low fraction of tagged copolymer with appreciably longer core-forming blocks and a high fraction of nontagged sample containing shorter core-forming blocks, the fluorometric measurements do not tell almost anything on the behavior of the pure nontagged sample, i.e., on the original micelles.

Conclusions

Extensive simulations of conformational characteristics of dense mixed systems of short and long self-avoiding chains enclosed in small spherical cavities and tethered to their surfaces yield data that help to understand the behavior of cores of mixed block copolymer micelles. The most important features of the conformational behavior of tethered chains may be summarized as follows:

1. In the central part of the cavity, the density of longer chains is higher than that of shorter chains. This apparently trivial finding is in fact complex and a rather indirect result of the behavior of mixed systems.

2. Dense systems of constrained tethered chains are generally very disordered and a high fraction of chains are oriented in a considerably oblique direction in respect to the radial direction. Their orientations (more precisely their $\mathbf{r}_{TF}$ vectors) decline more from the radial direction than those of longer chains. It is the result of the complex behavior of mixed constrained systems composed of tethered chains that are enclosed in small volumes.

3. Density of free ends of longer chains increases toward the core center, whereas that of short chains decreases. The pair distribution function of mutual distances of chain free ends is generally nonrandom and differs considerably for long and short chains.

4. Results of simulations indicate that great care should be taken when mixed micellar systems composed of tagged and nontagged chains are studied by fluorescence techniques. Both types of chains should be of the same length; otherwise results of fluorometric measurements may be considerably misleading.

Acknowledgment. This work was supported by Grants No. 203/97/0249 and 203/96/1381 (Grant Agency of the Czech Republic). The authors thank Dr. A. Yekta and Prof. M. I. Winnik from the University of Toronto, Ontario, Canada, and Prof. W. L. Mattice from the University of Akron, Akron, OH, for helpful discussions and suggestions.

Appendix

Comparison of the Directly Calculated Distribution Function of Pair Distances of Free Ends of Chains with That Recalculated from the Simulated Spatial Distribution of Free Ends within the Core on the Basis of the Mean Field Theory. A referee of the paper suggested we compare the directly simulated distribution function of free end distances with that obtained indirectly using arguments of the mean field approach. Such comparison is very useful since it reveals the significance of nontrivial interchain correlations that may exist in the spherically symmetrical system of tethered chains and that are not taken into account explicitly in the mean field approach. The comparison for homogeneous systems for different combinations of N and L (average segment density 0.55, radius of the cavity, $R = 10l$) is shown in Figure 9a, and the corresponding comparison for mixed systems studied in this paper is shown in Figure 9b.

The comparison allows us to draw the following conclusion. The number fractions of long end-to-end pair distances calculated using the mean field approach correspond well to those obtained directly. However, the mean field approach overestimates the number fractions of pairs with short distances. In our opinion, this discrepancy is due to the fact that the mean field approach does not take into account the fact that at least one of the neighbor lattice positions around the free end of the chain has to be necessarily occupied by the next (i.e., by the covalently bound) segment of this chain. Therefore, the probability of occupancy of closely located lattice sites by segments of the same chain increases for strongly coiled chain conformations that prevail in the strongly geometrically constrained system of tethered chains.

Nonradiative energy transfer and migration are very sensitive to the changes in numbers of closely located pairs of fluorophores. In systems with fluorophores attached at the ends of chains, the use of the mean field approach may lead to nonnegligible errors in calculations of fluorometric functions.

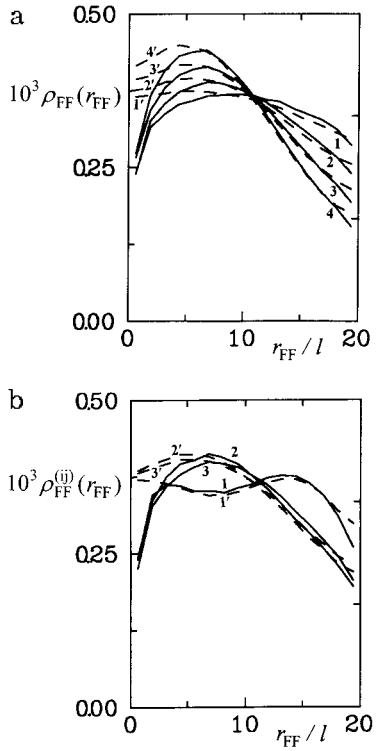

Figure 9. (a) Normalized pair distribution functions $\rho_{FF}(r_{FF})$ in the system composed of N tethered chains, each containing L segments: $N/L = 15/112$ (1), 25/67 (2), 35/48 (3), 45/37 (4). Radius of the cavity $R = 10l$, and the segment density is 0.6. Full curves represent simulated functions, and dashed curves with numbers with prime, the functions obtained by the mean the field approach. (b) Normalized pair distribution functions $\rho_{FF}^{(ij)}(r_{FF})$ in the system composed of 15 chains of the length $L = 80$ and 15 chains of the length $L = 20$. The segment density is 0.55, and radius of the cavity $R = 10l$. Full curves represent the simulated function $\rho_{FF}^{(11)}(r_{FF})$ for short chains (1), function $\rho_{FF}^{(22)}(r_{FF})$ for long chains (2), and distribution function of mutual distances of ends of short and long chains $\rho_{FF}^{(12)}(r_{FF})$ (3); dashed curves with numbers with prime are the corresponding functions obtained by the mean field approach.

References and Notes

(1) Tuzar, Z.; Kratochvil, P. In *Surface and Colloid Science*; Matijevic, E., Ed; Plenum Press: New York, 1993; Vol. 15.
(2) Ellias, H.-G.; Bareiss, R. *Chimia* **1967**, *21*, 53.
(3) (a) Leibler, L.; Orland, H.; Wheeler, J. C. *J. Chem. Phys.* **1983**, *79*, 3550. (b) Noolandi, J.; Hong, M. H. *Macromolecules* **1983**, *16*, 1443. (c) Whitmore, D.; Noolandi, J. *Macromolecules* **1985**, *18*, 657. (d) Meier, D. J. *J. Polym. Sci.* **1969**, *C26*, 81. (e) Helfland, E.; Tagami, Y. *J. Polym. Sci.* **1971**, *B9*, 741. (f) Helfland, E.; Sapse, A. M. *J. Chem. Phys.* **1975**, *62*, 1327. (g) Nagarajan, R.; Ganesh, K. *J. Chem. Phys.* **1989**, *90*, 5843. (h) ten Brinke, G.; Hadziioannou, G. *Macromolecules* **1987**, *20*, 486. (i) Halperin, A. *Macromolecules* **1987**, *20*, 2943. (j) Halperin, A.; Tirrell, M.; Lodge, T. P. *Adv. Polym. Sci.* **1991**, *100*, 31. (k) Dan, M.; Tirrell, M. *Macromolecules* **1993**, *26*, 4310. (l) Linse, P.; Malmstren, M. *Macromolecules* **1992**, *25*, 5434. (m) Linse, P. *Macromolecules* **1993**, *26*, 4437. (n) Linse, P. *Macromolecules* **1994**, *27*, 2685. (o) Linse, P. *Macromolecules* **1994**, *27*, 6404. (p) Hurter, P. N.; Scheutjens, J. M. H. M.; Hatton, T. A. *Macromolecules* **1993**, *26*, 5030, 5592. (q) Gruen, D. *J. Phys. Chem.* **1985**, *89*, 146, 153. (r) Ben-Shaul, A.; Szleifer, I.; Gelbart, W. M. *J. Chem. Phys.* **1985**, *83*, 3597. (s) Szleifer, I.; Ben-Shaul, A.; Gelbart, W. M. *J. Chem. Phys.* **1985**, *83*, 3612; **1986**, *85*, 5345; **1987**, *86*, 7094.
(4) Smit, B.; Esseling, K. S.; Hilberts, P. A. J.; van Os, N. M.; Rupert, L. A. M.; Szleifer, I. *Langmuir* **1993**, *9*, 9.
(5) (a) Owenson, B.; Pratt, L. R. *J. Phys. Chem.* **1984**, *88*, 2905, 6048. (b) Rodriques, K.; Mattice, W. L. *Polym. Bull.* **1991**, *25*, 239. (c) Rodriques, K.; Mattice, W. L. *J. Chem. Phys.* **1991**,

94, 761. (d) Rodriques, K.; Mattice, W. L. *Langmuir* **1992**, *8*, 456. (e) Wang, Y.; Mattice, W. L.; Napper, D. H. *Macromolecules* **1992**, *25*, 4073. (f) Wang, Y.; Mattice, W. L.; Napper, D. H. *Langmuir* **1993**, *9*, 66. (g) Adriani, P.; Wang, Y.; Mattice, W. L. *J. Chem. Phys.* **1994**, *100*, 7718. (h) Nguyen-Misra, M.; Mattice, W. L. *Macromolecules* **1995**, *28*, 1444; **1995**, 28, 6976. (i) Wijmans, C. M.; Linse, P. *Langmuir* **1995**, *11*, 3748.

(6) Grest, S. G.; Murat, M. In *Monte Carlo and Molecular Dynamics Simulation in Polymer Science*; Binder, K., Ed.; Oxford University Press: New York, 1995 (see also the references cited therein).

(7) (a) de Gennes, P.-G. *C. R. Acad. Sci. (Paris)* **1985**, *300*, 839. (b) Alexander, S. N. *J. Phys. (Paris)* **1977**, *38*, 983. (c) Milner, S. T.; Witten, T. A.; Cates, M. E. *Macromolecules* **1989**, *22*, 853. (d) Ball, R. C.; Marko, J. F.; Milner, S. T.; Witten, T. A. *Macromolecules* **1991**, *24*, 693. (e) Semenov, A. N. *Sov. Phys. JETP* **1985**, *61*, 733. (f) Birsthein, T. M.; Zhulina, E. B. *Polymer* **1989**, *30*, 170. (g) Zhulina, E. B.; Borisov, O. V.; Pryamitsyn, V. A.; Birshtein, T. M. *Macromolecules* **1991**, *24*, 140. (h) Zhulina, E. B.; Lyatskaya, Yu. V.; Birshtein, T. M. *Polymer* **1992**, *33*, 332.

(8) (a) Auroy, P.; Auvray L.; Leger L. *Macromolecules* **1991**, *24*, 5158. (b) Taunton, H. J.; Toprakcioglu, C.; Fetters, L. J.; Klein, J. *Nature* **1988**, *332*, 712. (c) Patel S. S.; Tirrel, M. *Annu. Rev. Phys. Chem.* **1989**, *40*, 597. (d) Gast, A. P.; Munch, M. R. *Polym. Commun.* **1989**, *30*, 324. (e) Parsonage, E.; Tirrel, M.; Watanabe, H.; Nuzzo, R. G. *Macromolecules* **1991**, *24*, 1987. (f) Granick, S.; Herz, J. *Macromolecules* **1985**, *18*, 460.

(9) (a) Stacy, C. J.; Kraus, G. *Polym. Eng Sci.* **1977**, *17*, 627. (b) Stacy, C. J.; Kraus, G. *Polym. Prepr. (Am. Chem. Soc., Div. Polym. Chem.)* **1977**, *18*, 323. (c) Pacovská, M.; Procházka, K.; Tuzar, Z.; Munk, P. *Polymer* **1993**, *34*, 4585. (d) Tian, M.; Qin, A.; Ramireddy, C.; Webber, S. E.; Munk, P.; Tuzar, Z.; Procházka, K. *Langmuir* **1993**, *9*, 1741.

(10) (a) Procházka, K.; Bednář, B.; Mukhtar, E.; Svoboda, P.; Trněná, J.; Almgren, M. *J. Phys. Chem.* **1991**, *55*, 4563. (b) Cao, T.; Munk, P.; Ramireddy, C.; Tuzar, Z.; Webber S. E. *Macromolecules* **1992**, *25*, 6300. (c) Ramireddy, C.; Tuzar, Z.; Procházka, K.; Webber, S. E.; Munk, P. *Macromolecules* **1992**, *25*, 2541. (d) Procházka, K.; Kiserow, D.; Ramireddy, C.; Tuzar, Z.; Munk, P.; Webber, S. E. *Macromolecules* **1992**, *25*, 454. (e) Kiserow, D.; Procházka, K.; Ramireddy, C.; Tuzar, Z.; Munk, P.; Webber, S. E. *Macromolecules* **1992**, *25*, 461. (f) Procházka, K.; Webber, S., E.; Munk, P. *J. Fluorescence* **1994**, *4*, 353.

(11) (a) Limpouchová, Z.; Procházka, K. *Collect. Czech. Chem. Commun.* **1993**, *58*, 2290. (b) Procházka, K.; Limpouchová, Z. *Collect. Czech. Chem. Commun.* **1994**, *59*, 782. (c) Limpouchová, Z.; Procházka, K. *Collect. Czech. Chem. Commun.* **1994**, *59*, 803. (d) Procházka, K.; Limpouchová, Z. *Collect. Czech. Chem. Commun.* **1994**, *59*, 2166. (e) Procházka, K. *J. Phys. Chem.* **1995**, *99*, 14108.

(12) (a) Allen, M. P.; Tildesley, D. J. *Computer Simulation of Liquids;* Clarendon Press: London, 1987 (reprinted: New York, 1993). (b) Kremer, K.; Binder, K. *Comput. Phys. Rep.* **1988**, *7*, 259. (c) Kremer, K.; Grest, G. S. *J. Chem. Soc., Faraday Trans.* **1992**, *88*, 1707.

(13) Rosenbluth, M. N.; Rosenbluth, A. W. *J. Chem. Phys.* **1955**, *23*, 356.

(14) Metropolis, N.; Rosenbluth, M. N.; Rosenbluth, A. W.; Teller, H. *J: Chem. Phys.* **1953**, *21*, 1087.

(15) Press, W. H.; Teukolsky, S. A.; Vettering, W. T.; Flannery, B. P. *Numerical Recipes in Fortran,* 2nd ed.; Cambridge University Press: Cambridge, U.K., 1992.

(16) Siepmann, J. I.; Frenkel, D. *Mol. Phys.* **1992**, *75*, 59.

(17) (a) Casassa, E. F. *Polym. Lett.* **1967**, *5*, 773. (b) Edwards, S. F. In *Molecular Fluids*; Ballian, R. Weill, G., Eds.; Gordon and Breach Science Publishers: London, 1974. (c) de Gennes, P. G. *Scaling Concepts in Polymer Physics*; Cornell University Press: Ithaca, NY, 1979. (d) Teraoka, I. In *Progress in Polymer Science*; Vogl, O., Jaycox, G. D., Vogl, J. C., Eds.; Elsevier Science: Oxford, U.K., 1996; Vol. 21 (see also the references cited therein). (e) Dayantis, J.; Sturm, J. *Polymer* **1985**, *26*, 1631. (f) DiMarzio, E. A.; Rubin, R. J. *J. Chem. Phys.* **1971**, *55*, 4318. (g) Wall, F. T.; Mandel, F.; Chin, J. C. *J. Chem. Phys.* **1976**, *65*, 2231. (h) Wall, F. T.; Chin, J. C.; Mandel, F. *J. Chem. Phys.* **1977**, *66*, 3066. (i) Gaylord, R. J.; Lohse, D. J. *J. Chem. Phys.* **1976**, *65*, 2779.

(18) Cheng, P.-L.; Berney, V. C.; Cohen, R. E. *Macromolecules* **1988**, *21*, 3442.

MA970001K